International Journal on Magnetic Particle Imaging
Vol 9, No 1, Suppl 1, Article ID 2303083, 4 Pages

Infinite Science Publishing

Proceedings Article

A Simulation Study for an Open-Sided Hybrid MPI-MRI Scanner

Sefa Karaca [a,b,c,*] · Damla Alptekin Soydan [a] · Can Barış Top [a,†] · Emine Ulku Saritas [b,c,†]

[a] ASELSAN Research Center, Aselsan A.Ş., Ankara, Turkey
[b] Electrical and Electronics Engineering, Bilkent University, Ankara, Turkey
[c] National Magnetic Resonance Research Center (UMRAM), Bilkent University, Ankara, Turkey
[†] Shared senior authorship
[*] Corresponding author, email: sefakaraca@aselsan.com.tr

Abstract

Magnetic particle imaging (MPI) provides images of magnetic nanoparticle distribution without any signal from the surrounding tissue. MPI would benefit from an additional imaging technique that reveals the anatomical background information, required in many applications. Here, we present a simulation study based on our in-house open-sided prototype MPI system, in which the coils can be utilized interchangeably for MPI and MRI data acquisitions. The system can provide a selection field gradient of 0.5 T m^{-1} for MPI in field free line topology, and a B_0 field of up to 50 mT for MRI. We analyze the system-induced deviations on MRI images for different B_0 values and pulse sequence parameters.

I. Introduction

In Magnetic Particle Imaging (MPI), spatial distribution of magnetic nanoparticles (MNPs) is imaged with high sensitivity and contrast [1]. However, anatomical background information via another imaging modality is needed to determine where the MNPs are relative to the human body. Considering that MPI does not use any ionizing radiation, combining it with another non-ionizing imaging modality is highly preferable. Previous work combined MPI and Magnetic Resonance Imaging (MRI) using standalone [2] and hybrid systems [3–6]. Fusion of images from separate MPI and MRI systems may not be a preferred solution in practice due to patient movement-related artifacts in the overlaid images. Hybrid MPI-MRI systems can potentially overcome this problem. Previously proposed hybrid systems employed close-bore configurations, which have high magnetic field efficiency, but may prohibit patient access and cause patient discomfort such as claustrophobia.

Recently, an open-sided MPI scanner capable of electronically scanning a field-free-line (FFL) was proposed [7]. The performance of the prototype system was analyzed via both simulations [8, 9] and experiments [10].

In this work, we present an open-sided hybrid MPI-MRI scanner, based on the aforementioned prototype system. The system features an MPI mode with FFL topology with 0.5 T m^{-1} selection field gradient and a low-field MRI mode with 5 mT - 50 mT B_0 field. Using simulations, we analyze the MRI performance of the hybrid system for different B_0 fields and pulse sequence parameters.

10.18416/ijmpi.2023.2303083

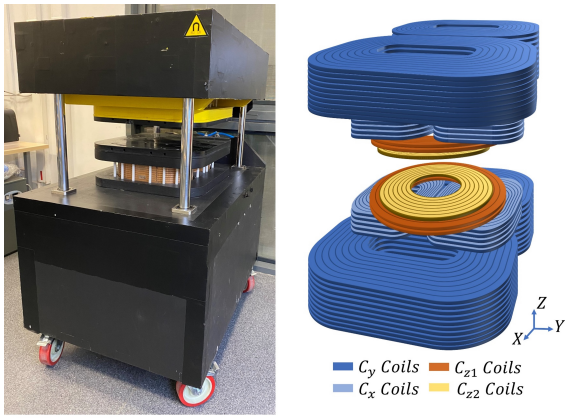

(a) (b)

Coil Group	Magnetic Particle Imaging		Magnetic Resonance Imaging	
	Purpose	Applied Field	Purpose	Applied Field
C_x	Selection Field	500 mT/m	Gradient Field (Y)	90 mT/m
C_y	Selection Field	500 mT/m	Gradient Field (X)	90 mT/m
C_{z1}	Focus Field	-*	Main Static Field	5 mT – 50 mT
C_{z2}	Drive Field	6.25 mT	Gradient Field (Z)	3 mT/m

(c)

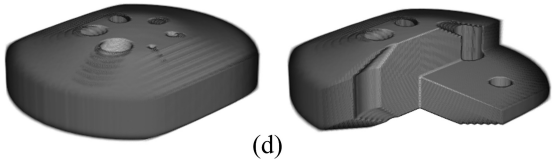

(d)

Figure 1: (a) Open-sided prototype ASELSAN MPI system and (b) its coil topology. The Tx/Rx coil of MRI and the receive coil of MPI are assumed to be ideal (not shown). (c) Function of each coil group for MPI and MRI modes for hybrid imaging. The listed applied field values are conservative. (d) 3D model of the designed bimodal phantom. The base material is modeled to mimic grey matter T1/T2 relaxation parameters in MRI. The vacancies are modeled to contain MNPs to be imaged via MPI.

II. Methods and Materials

II.I. Coil Topology for Hybrid System

The coil topology of the proposed hybrid system is modeled according to the specifications of the ASELSAN MPI prototype system [7]. Figure 1(a)-(b) shows the prototype system and the coil configuration. The functions of the different coil groups for both the MPI and MRI modes are listed in figure 1(c). A Helmholtz configuration coil group, denoted as C_{z1}, generates the *focus field* in MPI mode, and generates the B_0 field in MRI mode. The two bi-planar gradient coil groups, denoted as C_x and C_y, generate the magnetic field gradients in the x- and y-directions, respectively, for the selection field of MPI in FFL topology. These coils are also used to form the *gradient fields* in y- and x-directions in MRI mode. Another coil group, denoted as C_{z2}, generates the *drive field* in MPI mode when coils are fed in-phase; and generates the *gradient field* in z-direction in MRI mode when coils are fed out-of-phase.

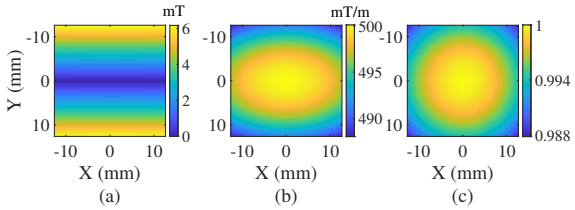

Figure 2: (a) B-field magnitude (B_z) of C_x coil group at $z=0$ plane, showing the formation of an FFL along the x-direction. (b) The gradient field magnitude ($\frac{\partial B_z}{\partial y}$) of C_x coil group at $z=0$ plane. A 0.5 T m^{-1} gradient field is created homogeneously. (c) Normalized B-field (B_z) for C_{z1} coil group at $z=0$ plane. The inhomogeneity value for the targeted FOV is 6000 ppm.

II.II. Simulations

For numerical simulations, a bimodal phantom given in figure 1(d) was designed. For a FOV of 25×25×15 mm^3, discretized with 0.2×0.2×0.2 mm^3 cells, the magnetic field maps of the coils (see figure 2) were computed using Maxwell (Ansys Electromagnetics Suite, Ansys Inc., USA), and then imported into in-house MPI and MRI simulators developed in MATLAB. Importantly, the inhomogeneity of the C_{z1} coil (i.e., B_0 field in MRI mode) was approximately 6000 parts-per-million (ppm). MPI receive coil and MRI Tx/Rx coils were assumed to be ideal.

For the MRI simulations, Bloch equations were applied on the magnetic moment vectors assigned to each cell, to simulate the T1/T2 relaxations, rotations due to RF pulses and gradients, and off-resonance effects. For a spin-echo pulse sequence, imaging parameters were chosen as 0.3 mm in-plane resolution and 2 mm slice thickness. To observe the system-induced deviations, simulations were carried out for B_0 ranging between 5 mT and 50 mT for MRI mode. The upper limit of 50 mT for B_0 was chosen based on initial feasibility simulations in Maxwell. To demonstrate the trade-offs in choosing B_0, the effects of noise were incorporated. Accordingly, zero-mean white Gaussian noise was added to k-space data, with standard deviation set to yield 15 dB signal-to-noise ratio (SNR) at $B_0 = 20$ mT and readout bandwidth of $BW = 100$ kHz. The SNR was then scaled with $B_0^{7/4} \cdot BW^{-1/2}$ for other B_0 and BW settings [11]. Image reconstruction was done via inverse 2D Fourier transform of the k-space data.

For MPI simulations, 0.5 T m^{-1} selection field and 6.25 mT-peak drive field at 25 kHz were applied. The received signal was modeled according to the MPI signal equation [12]. Noise was not incorporated in these simulations, as the operating settings of the MPI system were kept fixed. Images were reconstructed using the Kaczmarz algorithm [9].

10.18416/ijmpi.2023.2303083

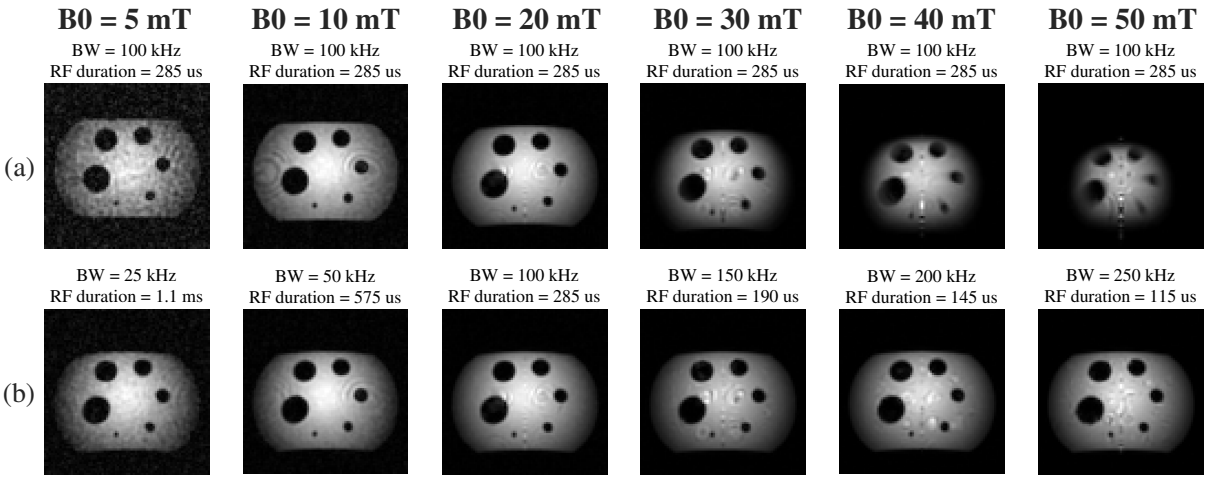

Figure 3: Reconstructed MRI images at different B_0 values (a) under identical RF duration and BW, and (b) for RF duration and BW rescaled to induce identical off-resonance effects at different B_0 values.

III. Results and Discussion

In figure 3(a), the reconstructed MRI images are shown for different B_0 values. When pulse sequence parameters (i.e., RF pulse duration and BW) are kept constant, low B_0 causes noisy reconstructions, whereas high B_0 causes severe signal dephasing and geometric distortions due to increased off-resonance effects. Next, RF pulse duration was reduced and BW was increased according to B_0, such that identical off-resonance effects are induced at different B_0 values. The limits of the RF pulse duration and BW used in the simulations were selected based on the experimental values in the literature [13, 14]. The reconstruction results in figure 3(b) show that for this scenario, SNR still increases with B_0 and image quality is maintained even at higher B_0 values. In practice, maximum feasible B_0 value depends on hardware limits for RF pulse duration and BW.

Finally, the overlaid image obtained with $B_0 = 20$ mT for the current hybrid system are compared with that from an ideal hybrid system in figure 4. The MRI image from the current system displays off-resonance induced geometric warping, which can be easily fixed with unwarping methods. Future studies will involve the design of a shimming coil to reduce B_0 *field* inhomogeneity and to allow a larger FOV in MRI mode.

IV. Conclusion

In this study, we presented a simulation study of an open-sided hybrid MPI-MRI scanner, in which the coils can be used interchangeably. The results indicate that the current system is adequate for performing MPI and low-field MRI with a proper selection of B_0 magnitude, RF pulse duration, and bandwidth.

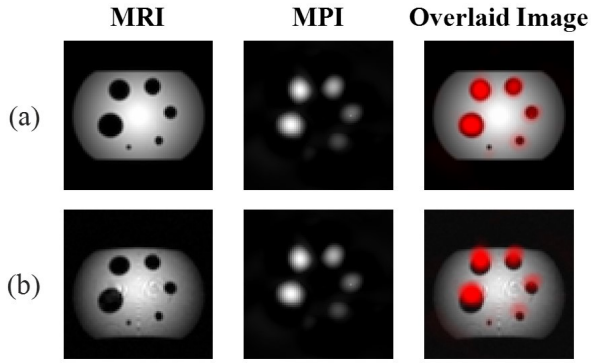

Figure 4: Reconstructed images for (a) ideal (i.e., with field inhomogeneities neglected) and (b) current hybrid systems for MRI mode (at $B_0 = 20$ mT) and MPI modes, together with the overlaid images.

Author's statement

Conflict of interest: EUS states no conflict of interest. SK, DAS, and CBT are employees of Aselsan A.Ş.

References

[1] B. Gleich and J. Weizenecker. Tomographic imaging using the nonlinear response of magnetic particles. *Nature*, 435(7046):1214–1217, 2005, doi:10.1038/nature03808.

[2] J. Weizenecker, B. Gleich, J. Rahmer, H. Dahnke, and J. Borgert. Three-dimensional real-time in vivo magnetic particle imaging. *Physics in Medicine & Biology*, 54(5):L1, 2009.

[3] J. Franke, U. Heinen, L. Matthies, V. Niemann, F. Jaspard, M. Heidenreich, and T. Buzug, First hybrid mpi-mri imaging system as integrated design for mice and rats: Description of the instrumentation setup, in *2013 International Workshop on Magnetic Particle Imaging (IWMPI)*, IEEE, 1–1, 2013.

[4] P. Vogel, S. Lother, M. A. Rückert, W. H. Kullmann, P. M. Jakob, F. Fidler, and V. C. Behr. Mri meets mpi: A bimodal mpi-mri tomograph. *IEEE Transactions on Medical Imaging*, 33(10):1954–1959, 2014.

[5] P. Klauer, P. Vogel, M. A. Rückert, W. H. Kullmann, P. M. Jakob, and V. C. Behr. Bimodal twmpi-mri hybrid scanner - coil setup and electronics. *IEEE Transactions on Magnetics*, 51(2):1–4, 2015.

[6] J. Franke, U. Heinen, H. Lehr, A. Weber, F. Jaspard, W. Ruhm, M. Heidenreich, and V. Schulz. System characterization of a highly integrated preclinical hybrid mpi-mri scanner. *IEEE Transactions on Medical Imaging*, 35(9):1993–2004, 2016.

[7] C. B. Top, S. Ilbey, and H. E. Güven. Electronically rotated and translated field-free line generation for open bore magnetic particle imaging. *Medical Physics*, 44(12):6225–6238, 2017.

[8] C. B. Top, A. Güngör, S. Ilbey, and H. E. Güven. Trajectory analysis for field free line magnetic particle imaging. *Medical Physics*, 46(4):1592–1607, 2019.

[9] D. A. Soydan, A. Güngör, and C. B. Top, A simulation study for three dimensional tomographic field free line magnetic particle imaging, in *2021 43rd Annual International Conference of the IEEE Engineering in Medicine & Biology Society (EMBC)*, IEEE, 3701–3704, 2021.

[10] C. B. Top and A. Güngör. Tomographic field free line magnetic particle imaging with an open-sided scanner configuration. *IEEE Transactions on Medical Imaging*, 39(12):4164–4173, 2020.

[11] D. G. Nishimura, Principles of magnetic resonance imaging. Stanford University, 1996,

[12] T. Knopp and T. M. Buzug, Magnetic Particle Imaging: An Introduction to Imaging Principles and Scanner Instrumentation, en. Berlin Heidelberg: Springer-Verlag, 2012, ISBN: 978-3-642-04198-3.

[13] T. O'Reilly, W. Teeuwisse, and A. Webb. Three-dimensional mri in a homogenous 27 cm diameter bore halbach array magnet. *Journal of Magnetic Resonance*, 307:106578, 2019, doi:10.1016/j.jmr.2019.106578.

[14] F. Illerstam, Quality assurance of the spatial accuracy of large field of view magnetic resonance imaging, 2014.

